nature physics

Article

https://doi.org/10.1038/s41567-023-02243-9

Non-affine atomic rearrangement of glasses through stress-induced structural anisotropy

Received: 2 October 2022

Accepted: 23 August 2023

Published online: 12 October 2023

Check for updates

Jie Dong[1,2,9], Hailong Peng[3,9] ✉, Hui Wang[4,9], Yang Tong[5] ✉, Yutian Wang[1,6], Wojciech Dmowski[4], Takeshi Egami[4,7,8], Baoan Sun[1,2,6] ✉, Weihua Wang[1,2,6] & Haiyang Bai[1,2,6] ✉

The atomic-scale structural rearrangement of glasses on applied stress is central to the understanding of their macroscopic mechanical properties and behaviour. However, experimentally resolving the atomic-scale structural changes of a deformed glass remains challenging due to the disordered nature of the glass structure. Conventional structural analyses such as X-ray diffraction are based on the assumption of structural isotropy and hence cannot discern the subtle atomic-scale structural rearrangement induced by deformation. Here we show that structural anisotropy correlates with non-affine atomic displacements—meaning those that do not preserve parallel lines in the atomic structure—in various types of glass. This serves as an approach for identifying the atomic-scale non-affine deformation in glasses. We also uncover the atomic-level mechanism responsible for plastic flow, which differs between metallic glasses and covalent glasses. The non-affine structural rearrangements in metallic glasses are mediated through the stretching or contraction of atomic bonds. The non-affinity of covalent glasses that occurs in a less localized manner is mediated through the rotation of atomic bonds or chains without changing the bond length. These findings provide key ingredients for exploring the atomic-scale process governing the macroscopic deformation of amorphous solids.

Glasses cover various kinds of vitrified solid including oxide glasses, polymer glasses and metallic glasses (MGs), which have been an indispensable part of our daily life and modern world[1]. Compared with crystalline materials, glassy materials exhibit remarkably different deformation behaviours[2–4]. For example, most glasses display high strength, yet tend to show strain localization on shear[5,6], and hence, they exhibit macroscopic brittle behaviour[7–9]. These deformation features are fundamentally related to the unique atomic-scale deformation mechanism of glasses for which the lattice defects do not exist in the amorphous structure[10–12]. Over the past decades, numerous atomic simulations have shown that the plastic flow in glasses at the atomic scale involves local non-affine structural rearrangement at defect-like regions[13–16]. Many theories were proposed based on this atomistic picture, including the free volume model[17], shear transformation zone

[1]Institute of Physics, Chinese Academy of Sciences, Beijing, China. [2]Songshan Lake Materials Laboratory, Dongguan, China. [3]School of Materials Science and Engineering, Central South University, Changsha, China. [4]Department of Materials Science and Engineering, University of Tennessee, Knoxville, TN, USA. [5]Institute for Advanced Studies in Precision Materials, Yantai University, Yantai, China. [6]College of Materials Science and Opto-Electronic Technology, University of Chinese Academy of Sciences, Beijing, China. [7]Department of Physics and Astronomy, University of Tennessee, Knoxville, TN, USA. [8]Materials Science and Technology Division, Oak Ridge National Laboratory, Oak Ridge, TN, USA. [9]These authors contributed equally: Jie Dong, Hailong Peng, Hui Wang. ✉e-mail: hailong.peng@csu.edu.cn; ytong1@utk.edu; sunba@iphy.ac.cn; hybai@iphy.ac.cn

model[18–20] and so on. The local non-affine structural rearrangement has also been experimentally identified in colloidal glasses[21–24] owing to the large length and long timescales of colloidal particles. However, experimentally resolving atomic-scale non-affine deformation in atomic or molecular glasses remains a substantial challenge. Furthermore, despite the success of local arrangement modelling, the identification of specific atomic mechanisms for different types of glass is still not fully achieved. For example, covalently bonded glasses exhibit plastic flow behaviour that notably differs from that of MGs[25,26]. The loosely packed or low-density atomic regions are susceptible to plastic flow and hence are often considered as 'plasticity carriers' in MGs[4,18]. In contrast, the high-density components are found to act as plasticity carriers responsible for the plastic flow in network-bonded silicon glass[25], which is opposite to the picture for MGs. We still lack a fundamental understanding of the atomistic origin of such contrasting behaviours, in terms of the atomic-level process responsible for the plastic flow in various types of glass.

Identifying the non-affine rearrangement from atomic displacement is crucial for understanding the mechanical failure of solids, melting of crystals and devitrification of glasses[14,19,27,28]. Currently, a paradigm utilizing the coarse-graining method has been proposed to decompose the atomic displacement into a decoupled affine and non-affine part by properly choosing the projection operator in the frame of the lattice structure[29]. This shows that non-affine displacement can originate from the spatial heterogeneity of elastic moduli[30] and thermal fluctuations[29]. The non-affine part also accounts for the emergence of defects or slip planes[28,31] and the metastable transition at infinitesimal stresses in crystals[32].

For deformed amorphous solids, the non-affinity of atomic displacement is related to the breaking of local centrosymmetry[27,33,34]. In a centrosymmetric crystalline lattice, the forces applied on any one atom are balanced by its pair nearest neighbours due to mirror symmetry or inversion symmetry[33]. This leads to the affine displacements of atoms, which are proportional to the applied deformation. However, in a disordered lattice, each atom is in a unique local configuration with the breaking of centrosymmetry. As a result, the forces applied to an atom cannot be cancelled out and have to be balanced by a non-affine displacement to ensure local mechanical equilibrium[21,33]. Recently, it has been shown that the non-affinity of atomic displacements is critical for understanding the softness of the elastic rigidity of amorphous solids[27,35,36] and hence the glass transition[33]. On the other hand, the amorphous structure of a glass or liquid on shear flow tends to be distorted from the spherical symmetry or becomes anisotropic[37,38]. The shear-induced structural anisotropy has been observed in the nonlinear rheology of liquids[39], as well as the deformation of polymer[40] and MGs[41–43], and can be described by the distortion of pair distribution functions (PDFs) in terms of spherical harmonic expansions[38,42], which contain key information about the atomic-level deformation process. Therefore, one can speculate that atomic non-affine deformation may leave some 'fingerprints' in the shear-induced structural anisotropy of a deformed glass.

In this study, we make a connection between the deformation-induced structural anisotropy and atomic non-affine deformation in various types of glass by high-energy X-ray diffraction (XRD). Through a quantitative analysis of anisotropic PDFs, we identify the specific mode for non-affine atomic deformation, which is different between MGs and the other types of glass of covalent bonds. The experimental results are also validated by atomistic simulations, providing atomic-level insights into the physical mechanism governing the macroscopic deformation of amorphous solids.

For anisotropic materials, the directional dependence of structural factors and PDFs can be well described by spherical harmonic expansions[41,42]:

$$S(\mathbf{Q}) = \sum_{l,m} S_l^m(Q)\, Y_l^m\left(\frac{\mathbf{Q}}{Q}\right), \qquad g(\mathbf{r}) = \sum_{l,m} g_l^m(r)\, Y_l^m\left(\frac{\mathbf{r}}{r}\right). \quad (1)$$

Here Y_l^m is the spherical harmonics, $\mathbf{r}$ is the distance vector and $\mathbf{Q}$ is the scattering vector. The coefficients of spherical harmonics $S_l^m(Q)$ and $g_l^m(r)$ contain information of the local structure change, and are related through the spherical Bessel transformation[42,44]:

$$g_l^m(r) = \frac{i^l}{2\pi^2\rho_0}\int S_l^m(Q) J_l(Qr)\, Q^2 \mathrm{d}Q, \quad (2)$$

where ρ_0 is the number density of atoms and $J_l(x)$ is the spherical Bessel function. Among these coefficients, $S_0^0(Q)$ and $g_0^0(r)$ represent the isotropic structural change on deformation, whereas the anisotropic structural factor and PDF, that is, $S_2^0(Q)$ and $g_2^0(r)$, reflect the structure difference between two perpendicular directions on uniaxial deformation[41]. Assuming that the sample is isotropic in the x–y plane, we have $m = 0$ and equations (1) and (2) can be simplified. In the case of uniaxial deformation, if only the terms up to $l = 2$ are considered, we have $S_2^0(Q) = (16\pi/45)^{1/2}[S(Q,\chi = 0) - S(Q,\chi = \pi/2)]$. Here χ is the angle between the sample anisotropy axis (the 'z axis') and the scattering vector $\mathbf{Q}$, which lies in the plane containing the 'z axis' (ref. 45). Therefore, the terms $S_2^0(Q)$ and $g_2^0(r)$ can be experimentally obtained from the diffraction experiments. For a glassy solid on affine deformation, it has been theoretically showed that the anisotropic PDF, $g_2^0(r)$, is proportional to the first derivative of the isotropic PDF for the first-order expansion with respect to the deformation strain[38,42,45]. For an elastic affine deformation in a uniaxial compression[44], $g_2^0(r)$ can be expressed in terms of $\mathrm{d}g(r)/\mathrm{d}r$:

$$g_{2,\mathrm{aff}}^0(r) = \varepsilon_{\mathrm{aff}}\left(\frac{1}{5}\right)^{1/2}\frac{2(1+\nu)}{3} r\frac{\mathrm{d}g(r)}{\mathrm{d}r}, \quad (3)$$

where ν is the Poisson ratio and $\varepsilon_{\mathrm{aff}}$ is the affine strain along the loading axis.

We chose four different types of glass for the experimental study: a MG ($Zr_{52.5}Cu_{17.9}Ni_{14.6}Al_{10}Ti_5$, Vit105), a polymer glass (polystyrene (PS)), a monatomic glass (amorphous Se) and an oxide glass (B_2O_3). These glasses were first annealed at a temperature of $0.9T_g$ (T_g is the glass transition temperature) and then subjected to the high-temperature creep treatment at $0.9T_g$ and a constant uniaxial compressive stress of $0.9\sigma_y$ (σ_y is the yield strength of the glass at $0.9T_g$). Methods provides more experimental details. After the creep treatment, independent high-energy XRD measurements were carried out along two orientations at room temperature (Fig. 1a). The first measurement was performed with the 'instrumental z axis' parallel to the loading axis of the crept samples (denoted as the P position). Then, the sample was in-plane (the y–z plane) rotated by 90° around the diffraction axis (denoted as the N position), and the measurement was repeated. Two-dimensional diffraction patterns of samples were collected for each position. Special care has been taken to reduce both instrumental and statistical errors (Methods), which is important for the accurate measurement of structural anisotropy signals. The existence of structural anisotropy in the crept samples can be justified by differencing the two-dimensional diffraction patterns between the P and N positions. Averaging these two patterns gives the isotropic structure, and the discrepancy between them gives the anisotropic one. For glassy materials with an isotropic structure, the circular diffraction rings obtained from two states cancel each other after the difference, whereas the diffraction rings from anisotropic glassy solids are distorted, not cancelling out after rotating 90°. Typical examples of differential diffraction patterns for both undeformed and high-temperature crept Vit105 MG samples are shown in Fig. 1b,c, respectively. Evidently, the undeformed sample has an ideal isotropic atomic structure with a homogeneous contrast on the differential diffraction pattern, whereas the high-temperature crept sample shows non-overlapped ellipse diffraction rings, indicating the existence of an anisotropic atomic structure. The same phenomenon

https://doi.org/10.1038/s41567-023-02243-9

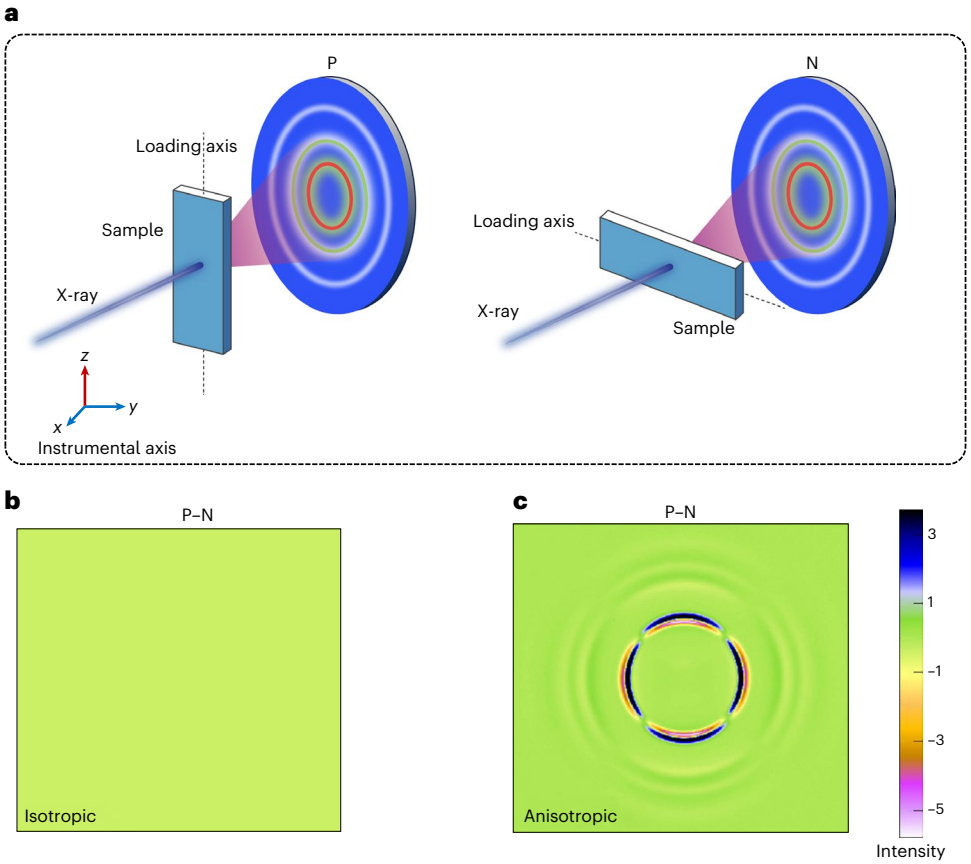

Fig. 1 | Illustration of detecting and characterizing the anisotropic structure for glasses after creep. a, Schematic of the XRD setup for detecting structural anisotropy. **b**, For the undeformed MG sample, the circular diffraction rings for the P and N positions are balanced with each other after differencing, indicating the isotropic structure. **c**, For the high-temperature crept MG sample, non-overlapped elliptical diffraction rings are observed after differencing the signals of P and N positions, indicating the anisotropic structure.

is also observed for other types of glass (Supplementary Fig. 1). These results suggest that the structural anisotropy is a general signature of glasses of various types as driven by the plastic deformation after the high-temperature creep.

Figure 2 (left) shows the anisotropic PDF $g^0_{2,\mathrm{exp}}(r)$ (solid line) obtained from experimental results for different types of glass. The affine part, $g^0_{2,\mathrm{aff}}(r)$ (Fig. 2 (left), dashed line), can also be extracted by fitting the experimental curves according to equation (3), with the fitting parameter $\alpha = \frac{2(1+\nu)}{3\sqrt{5}}\varepsilon_{\mathrm{aff}}$. The values of α fitted for different glasses are given in the figure. A comparison of the isotropic $g^0_{0,\mathrm{exp}}(r)$ and anisotropic $g^0_{2,\mathrm{exp}}(r)$ values is also shown (Fig. 2, right). For Vit105 MG (Fig. 2a), it is evident that $g^0_{2,\mathrm{exp}}(r)$ and $g^0_{2,\mathrm{aff}}(r)$ match well with each other at large interatomic distances ($r > 11$ Å), indicating an affine deformation at a long distance. At $r < 11$ Å, $g^0_{2,\mathrm{exp}}(r)$ and $g^0_{2,\mathrm{aff}}(r)$ are in phase, but $g^0_{2,\mathrm{exp}}(r)$ has a lower peak height than $g^0_{2,\mathrm{aff}}(r)$, indicating the occurrence of non-affine strain or inelastic strain at $r < 11$ Å. These results are similar to earlier reports[30,31,34], and imply that the MG deforms in a manner of the localized inelastic regions embedded in an elastic deformed matrix. The long-range affine strain observed here could originate from the 'frozen-in' anelasticity quenched from the high-temperature creep. According to previous studies[46], when the sample is cooled down and the stress is removed from the creep, the anelastic strain only recovers a little and most of the anelasticity is retained at room temperature, which produces long-range elastic stress in the matrix to balance the stress produced due to the constraint of local strained regions[44]. It is worth noting that equation (3) is just the first-order approximation in an infinite expansion for the two-point correlation function[38]. We also performed an error analysis of the higher-order terms for the MG (Supplementary Text I). The results clearly show that the first-order expansion is accurate enough for extracting $g^0_{2,\mathrm{aff}}(r)$, and the higher-order terms can be neglected for our experimental results.

The critical distance r_c at which $g^0_{2,\mathrm{exp}}(r)$ begins to deviate from $g^0_{2,\mathrm{aff}}(r)$ can be roughly taken as the characteristic size of local regions (or the radius if the region is spherical) undergoing non-affine deformation. The average size of the localized non-affine region determined for the MG by this way is around 1.1 nm, corresponding to hundreds of atoms. According to the literature, a single shear transformation zone usually contains 5–50 atoms[47,48]. Therefore, the local non-affine deformation of MGs determined by the structural anisotropic analysis may involve a cascade of or avalanche of several shear transformation zones. This is consistent with the results from atomistic simulations[48,49]. From Fig. 2b, one can see a clear shift in the peak positions in $g^0_{2,\mathrm{exp}}(r)$ relative to those in $g^0_{0,\mathrm{exp}}(r)$. This suggests a change in the coordinating distance around any atom during the deformation of the MG. Since the first nearest-neighbour peak of the PDF is relatively well separated from the second peak, the atomic-bond length in MGs can be roughly defined as the average distance between the nearest-neighbour atoms[42]. In this sense, we can see that the local non-affine atomic arrangements in MGs mainly proceed through the stretching or contraction of atomic bonds, probably accompanied by the breaking of some bonds.

It is interesting to test whether the microscopic deformation mechanism observed in MGs can be extended to other types of glass or not. For non-MGs (B_2O_3, Se and PS), the anisotropic profiles exhibit remarkable differences from those in MG. For Se, $g^0_{2,\mathrm{exp}}(r)$ and $g^0_{2,\mathrm{aff}}(r)$ show little resemblance (Fig. 2c). For B_2O_3 and PS, $g^0_{2,\mathrm{aff}}(r)$

https://doi.org/10.1038/s41567-023-02243-9

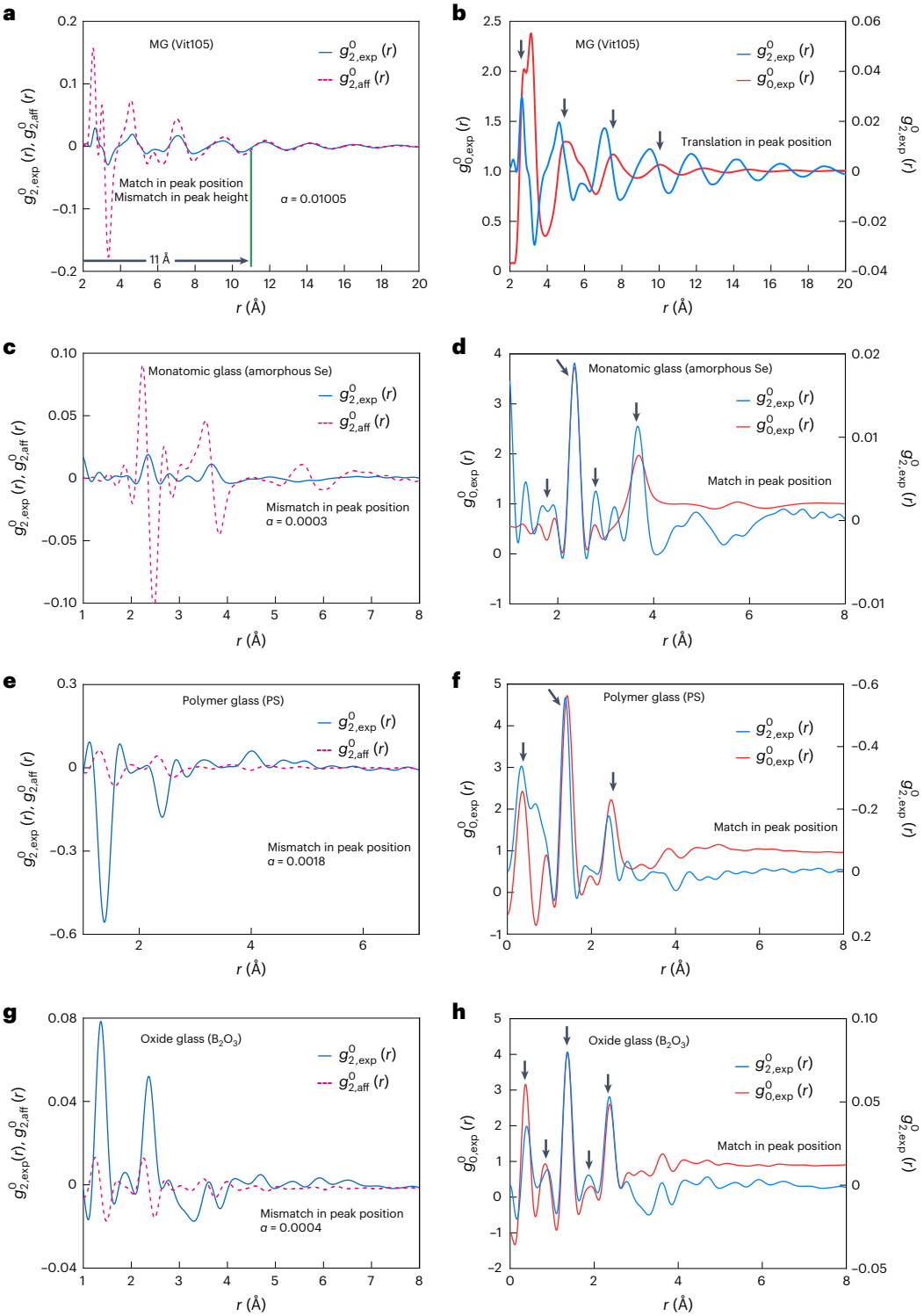

Fig. 2 | Comparison of experimentally observed anisotropic PDF to theoretically fitted anisotropic PDF, and to observed isotropic PDF for the studied glasses after creep deformation. Experimentally observed anisotropic PDF $g^0_{2,exp}(r)$, theoretically fitted anisotropic PDF $g^0_{2,aff}(r)$ and observed isotropic PDF $g^0_{0,exp}(r)$. **a**, For the Vit105 MG, $g^0_{2,exp}(r)$ matches well with $g^0_{2,aff}(r)$ at the long distance (>11 Å), but has a much lower peak height at the short distance (<11 Å). **b**, Shift in the peak position of $g^0_{2,exp}(r)$ relative to $g^0_{0,exp}(r)$, suggesting the change in bond length during deformation. **c**,**e**,**g**, Comparison of observed $g^0_{2,exp}(r)$ and theoretically fitted $g^0_{2,aff}(r)$ for amorphous Se (**c**), PS (**e**) and B_2O_3 (**g**) glass, respectively. The peak positions of $g^0_{2,exp}(r)$ and $g^0_{2,aff}(r)$ do not match in these glasses. **d**,**f**,**h**, Comparison of observed $g^0_{2,exp}(r)$ and $g^0_{0,exp}(r)$ for amorphous Se (**d**), PS (**f**) and B_2O_3 (**h**) glass, respectively. The good agreement in the peak positions between $g^0_{2,exp}(r)$ and $g^0_{0,exp}(r)$ in these glasses indicates the rotation of atomic bonds without changing the bond length.Source data

becomes almost flat beyond 5 Å, whereas $g^0_{2,exp}(r)$ shows some oscillations above 5 Å. The curves of $g^0_{2,exp}(r)$ and $g^0_{2,aff}(r)$ are clearly not matched with each other in the peak positions (Fig. 2e,g). This absence of similarity between $g^0_{2,exp}(r)$ and $g^0_{2,aff}(r)$ implies that the structural changes in these glasses are intrinsically non-affine. Even though they appear elastic at a macroscopic scale, at the atomic scale, they undergo non-affine rearrangement on the anelastic deformation. Therefore, the mechanism of anelastic deformation of these glasses is

https://doi.org/10.1038/s41567-023-02243-9

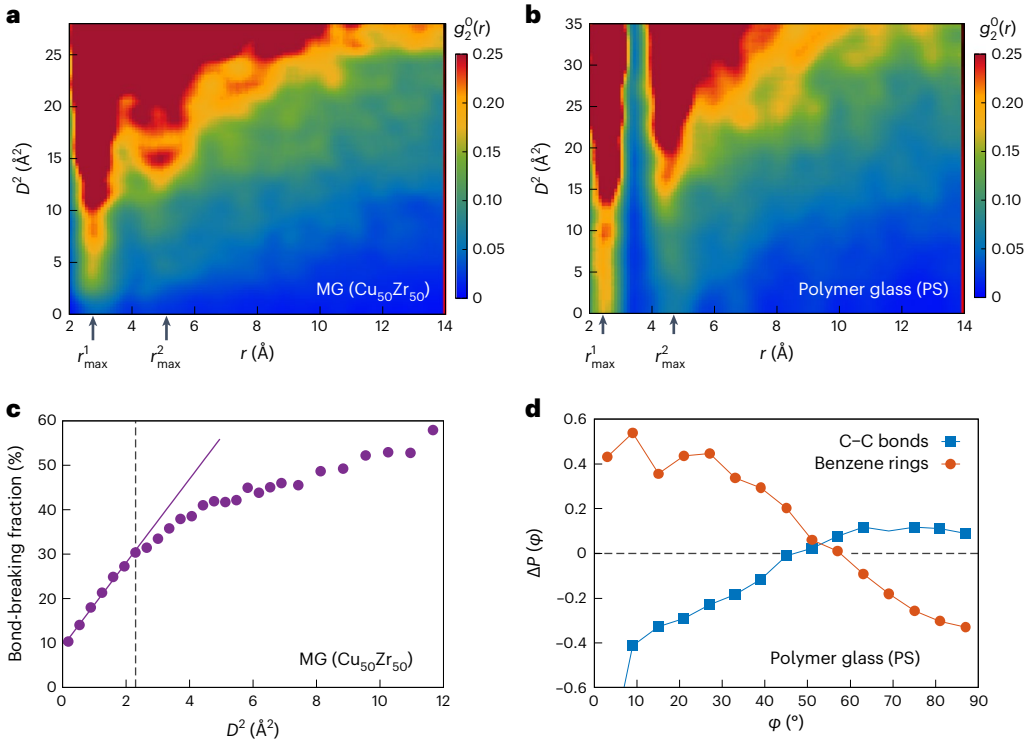

Fig. 3 | Correlations of structural anisotropy with non-affine deformation and changes in bonds for deformed metallic and polymer glasses in simulations. a,**b**, For both MG (**a**) and polymer (**b**) glass, the intensity of $g_2^0(r)$ increases with the squared non-affinity D^2 at any r, indicating a positive correlation between structural anisotropy and local non-affine deformation (r^1_{max} and r^2_{max} denote the first and second peak positions in $g(r)$, respectively). **c**, In the MG, the fraction of the number of breaking bonds increases with D^2, indicating a bond-cutting-mediated plastic deformation mechanism. **d**, For the polymer glass after creep, the angle probability distribution for the C–C bonds in the aliphatic moiety increases in the direction perpendicular to the compression axis ($\varphi > 45°$) on the expense of the probability in parallel directions ($\varphi < 45°$), whereas it is opposite for that of the benzene rings. This indicates the reorientation of C–C bonds towards the plane perpendicular to the compression axis in both cases, suggesting a bond-rotation-mediated deformation mechanism.Source data

fundamentally different from that of MGs. On the other hand, the comparison of $g^0_{2,exp}(r)$with $g^0_{0,exp}(r)$shows that their peaks are in phase (Fig. 2d,f,g (arrows) for B_2O_3, Se and PS glasses, respectively). This means that the bond lengths between atoms and interchain distances in these glasses do not change during the local non-affine atomic arrangements, suggesting that the structural changes occur mainly due to the rotation of atomic bonds, without changing the bond length.

By analysing the discrepancy between $g^0_{2,exp}(r)$ and $g^0_{2,aff}(r)$, many key information about the atomic-scale non-affine deformation can be extracted for different types of glass. Alternatively, we can also precisely determine the radially varying strain, $\varepsilon(r)$, from the experimentally measured $g^0_{2,exp}(r)$ and $g_{exp}(r)$ values based on the theoretical methods discussed in another work[36] (Supplementary Text II). Supplementary Fig. 4 shows the radially varying strain curves of $\varepsilon(r)$ for the Vit105 MG solved for both first-order and second-order approximations. The spatially dependent non-affine strain $\varepsilon_{nonaff}(r)$ can be well distinguished from the constant affine strain ε_{aff}. We can clearly see that $\varepsilon_{nonaff}(r)$ violently oscillates at small r and gradually approaches ε_{aff} at large r, indicating that the non-affine deformation of MGs is spatially localized and tends to disappear at large distances. The separation of the non-affine part and affine part here is well consistent with the decomposition of microscopic particle displacements into non-affine and affine parts with the computational methods presented in the literature[19,29]. We also calculated the spatially dependent strain curves by artificially choosing different values of ε_{aff} (affine strain can be input as the initial value of $\varepsilon(r)$ at the large end of r) (Supplementary Fig. 5). Evidently, with the increase in ε_{aff}, $\varepsilon_{nonaff}(r)$ becomes stronger as indicated by the increased height of the peaks in $\varepsilon_{nonaff}(r)$, whereas the positions for the occurrence of non-affine strain are unchanged. Since the constant affine strain is the 'frozen-in' anelasticity quenched from the high-temperature creep[49], and is positively related to the macroscopic creep strain, the calculated results suggest that the non-affinity of atomic arrangements becomes stronger with the increase in macroscopic creep deformation.

To verify the experimental results, we performed molecular dynamics (MD) simulations on the creep of a typical MG ($Cu_{50}Zr_{50}$) and a covalently bonded polymer glass (PS). The creep curves and the comparison of $g^0_2(r)$ with $g^0_0(r)$ and $\alpha dg(r)/dr$ in the simulation agree well with that in the experiments (Supplementary Fig. 6). In the MD simulations, the non-affine structural rearrangement can be quantified by the squared mean of non-affine displacement, D^2, on a local level. Its calculation can be generalized as the projection of atomic displacement into mutually orthogonal subspaces using the projectors that depend on the coarse-grained volume[29]. The separated affine part represents the homogeneous linear transformations of a reference configuration within the coarse-grained volume, whereas the non-affine part represents the deviation from the linear response related with the defect generation in crystals or the emergence of a shear transformation zone in glasses[19,28,31]. The correlation functions concerning the affine and non-affine displacements can be computed for crystals within harmonic theory[29,31]. Here D^2 is defined as the squared deviation of the relative displacement of the nearest neighbours about the central atoms after creep to the affine transformation of the displacement field before creep, by choosing that the affine transformation minimizes the square of the deviation[3]. We calculated $g^0_2(r)$ for each particle and compared it with the squared non-affine

https://doi.org/10.1038/s41567-023-02243-9

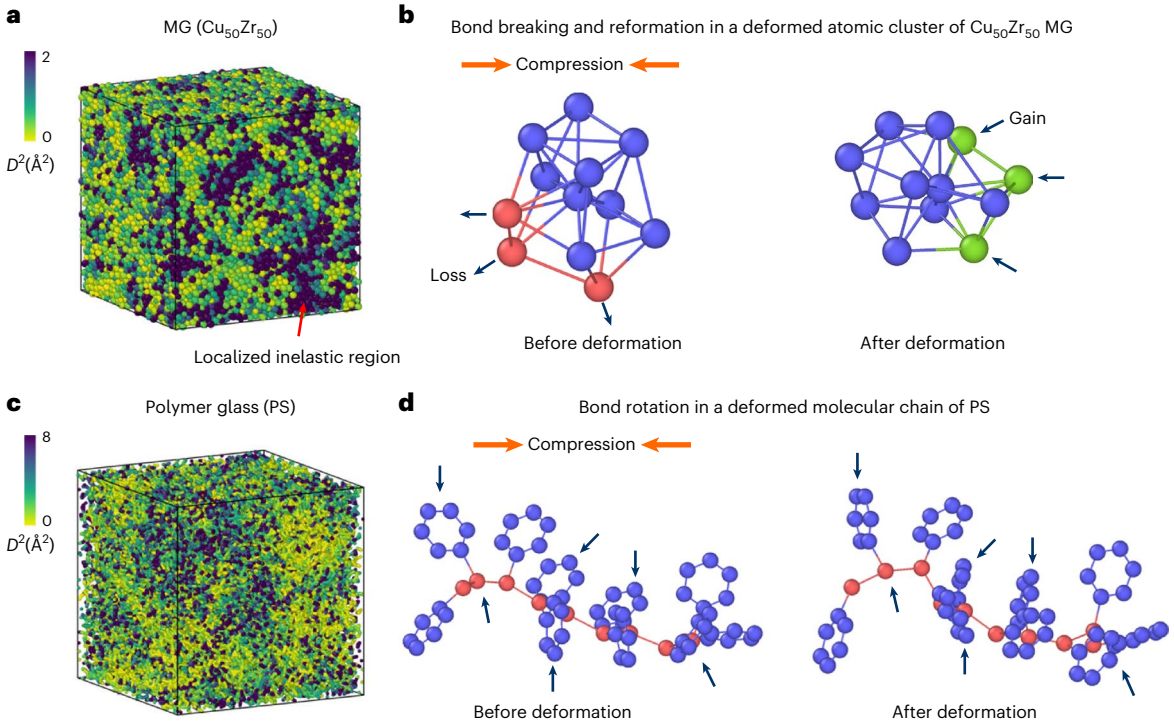

Fig. 4 | Unveiled deformation mechanisms of metallic and polymer glasses in simulations. a, Squared non-affine displacements (represented by the colour bar) in the simulated $Cu_{50}Zr_{50}$ MG revealing a heterogeneous deformation with severely deformed local plastic regions embedded in the elastic matrix. **b**, Deformed cluster of MG clearly showing changes in bond lengths, as well as the loss and gain of atoms via bond breaking and formation. **c**, Squared non-affine displacement (represented by the colour bar) in the simulated polymer glass is relatively uniform compared with that in the MG. **d**, After creep deformation, a chain of the simulated polymer glass clearly shows a reorientation of C–C bonds and benzene rings (obvious changes are denoted by the arrows).

displacement D^2 for the same particle. As shown in Fig. 3a,b, the magnitude of anisotropy increases with D^2 at any distance r, indicating that the atoms of higher non-affinity also exhibit stronger structural anisotropy. This correlation is more evident at the first- and second-nearest-neighbour shells (Fig. 3a,b, arrows labelled r^1_{max} and r^2_{max}). With increasing r, the onset position of clear anisotropy shifts to the larger D^2, suggesting that the spatial range of structural anisotropy monotonically depends on the strength of non-affine deformation. In Fig. 3, we chose the nearest neighbours as the cutoff in the D^2 calculation. This is due to the fact that this is the smallest length scale that the elasticity can be properly defined, and is of the highest precision for the property of the atomic attribute. We also checked the effect of the cutoff on the correlation by varying the cutoff for the D^2 calculation in the vicinity of the first neighbours, for example, $r_{cutoff} = 1.5r_{min}$, where r_{min} is the first minimum in $g(r)$ (Supplementary Fig. 7). The correlation between structural anisotropy and non-affine deformation (Supplementary Fig. 7) is similar to that shown in Fig. 3. We, thus, conclude that structural anisotropy is a good measure of the magnitude and spatial extension of local plasticity in both atomic and molecular glasses.

To elucidate the atomic-level deformation mechanism alluded by the experimental results, we analysed the bond breaking after the creep in MGs. If two atoms are separated by a distance less than the first minimum position in $g(r)$, they are considered to be bonded in MGs, and vice versa. The bond-breaking percentage for each particle, defined as the fraction of the number of broken bonds among the total bonds after creep, is averaged over the particle for each value of D^2 (Fig. 3c). The fraction of breaking bonds monotonically increases with D^2, exhibiting a linear relation at small squared non-affine displacement. This linear relation can also be verified in colloidal suspensions at a small value[23], confirming that the plasticity is conferred by the bond-breaking events in atomic systems. Interestingly, the linear fit hits the 'y axis' at a non-zero value, indicating a threshold of the bond-breaking percentage of about 10% for a plastic-flow event. As the average coordination number is around 12–14 in MGs, this means that at least one bond has to be broken around the central particle for the inelastic deformation to occur.

In polymer glasses, the relevant atomic motion is the rotation of covalent bonds. There are two kinds of carbon–carbon (C–C) bond in PS glasses: one is the C–C bond in the aliphatic moiety (the chain of C–C bonds that link the benzene rings in PS glass) characterized by its bond orientation, and the other one is the C–C bond in benzene rings characterized by the normal direction of the benzene rings. We calculated the distribution probability difference $\Delta P(\varphi)$, defined as the distribution probability difference of C–C bonds at angle φ before and after the creep. Here φ is the angle between the C–C-bond orientation and the compression axis, or the normal direction of benzene rings and compression axis. As shown in Fig. 3d, an enhanced probability can be seen at around $\varphi = 0°$ for the benzene rings, whereas the enhanced probability locates at around $\varphi = 90°$ for the C–C bonds in the aliphatic moiety. This gives the evidence that compression reorients the benzene rings and C–C bonds towards the plane perpendicular to stress, confirming that irreversible deformation is accomplished by the reorientation of covalent bonds in this molecular glass.

The intuitive atomic-level processes associated with plastic deformation in metallic and polymer glasses obtained from MD simulations are shown in Fig. 4. Plastic deformation represented by the squared non-affine displacement field is spatially heterogeneous both in metallic and polymer glasses (Fig. 4a,c). An intuitive deformation mechanism is shown in Fig. 4b,d that presents configuration changes in the deformation units of the simulated glasses. On compression, the local atomic structure in MG is plastically deformed with bond contraction and stretching (Fig. 4b), resulting in bond breaking and reformation denoted by arrows, thus losing and regaining the neighbour atoms. For the polymer glass, Fig. 4d shows a fairly different mechanism:

the molecular chain rotates, as denoted by arrows, without obvious changes in the bond length. The structural anisotropy of the samples after creep measured by diffraction clearly suggests these deformation mechanisms.

Currently, the general understanding of the deformation mechanism of atomic or molecular glasses is mainly achieved through theoretical models and simulations[17–19]. Experimentally resolving the atomic-scale deformation process of glasses with conventional techniques, such as electron microscopy, remains extremely challenging. Our results suggest that the deformation-induced structural anisotropy can act as a unique approach for identifying the atomic-scale non-affine deformation in real glassy materials: they reveal hidden information about their atomic-scale deformation process, and provide a 'fingerprint' of the deformation mechanism. The commonly proposed deformation 'order parameter' is usually based on the pre-knowledge of local packing geometry[19,50–52]. Our approach does not require any prior detailed knowledge of the atomic structure, rendering a direct measure of deformation. Our simulations demonstrate that the structural anisotropy correlates with the non-affine atomic displacement in a local manner, corroborating the intuitive interpretation of the experimental findings. Therefore, this approach allows direct access to the atomic-scale deformation information by diffraction experiments for samples that underwent creep deformation. Further, it is noted that the defects in crystalline materials are susceptible to non-affine atomic displacements[28,31], which is essential for understanding their macroscopical mechanical response. Our structural anisotropy approach to detect non-affine atomic displacements may be extended to crystalline solids with a high concentration of defects.

Based on the structural anisotropy analysis, we can see that the plastic flow of MGs proceeds in a manner of the localized inelastic regions embedded in an elastically deformed matrix. This picture is consistent with the local atomic rearranging models proposed[18,53,54]. The average size of the local inelastic regions determined for the MG from our analysis is ~1.1 nm, consistent with the estimation by the strain-rate jump experiments[47,48,55] and with earlier results[41]. On the other hand, the size of the local deformation unit is small, involving 5–50 atoms on average[42]. Thus, creep deformation must involve a cascade process associated with ductile deformation[43]. In contrast, a surprisingly long-range elastic field is not visible for covalent and polymer glasses. These glasses are not close packed but have more open structures. Thus, deformation occurs through the local rotation of chains and covalent units. Because of the complexity of the structure of the isotropic PDF, $g^0_{0,\mathrm{exp}}(r)$ quickly loses signal with distance, making the long-range stress field invisible to the PDF. A chemically resolved PDF may offer more information. It is interesting to note that $g^0_{2,\mathrm{exp}}(r)$ shows more oscillations than $g^0_{0,\mathrm{exp}}(r)$, and modelling this will help to understand the deformation mechanism better. Rotation of atomic bonds or molecular chains is consistent with the anomalous plastic flow behaviour observed in directionally bonded glasses[25,26]. In addition, the mode of non-affine atomic arrangements (stretching and contraction versus the rotation of atomic bonds) also has an important impact on the macroscopic creep behaviour of glasses (Supplementary Fig. 8). For the MG, the non-affine mode of atomic-bond stretching and contraction leads to a continuous and gradual increase in the creep strain with the creep time; the sample was finally crept into a barrel shape without rupture, indicating that the mode of bond stretching and contraction can sustain a large plastic deformation. However, for the polymer glass, the strain increases sharply at some time in the later creep stage, leading to the rupture of the sample. This suggests that the mode of rotation of atomic bonds has a limit for sustaining plastic deformation.

Finally, it is worth noting that stress-induced structural anisotropy leads to the anisotropy of properties in glasses[56]. We measured the elastic modulus E of the crept Vit105 MG rod across the cross section and longitudinal section (Supplementary Fig. 9). The average E value for the two sections is 102 and 110 GPa, respectively, with a difference of ~7.8%. Such an obvious difference in E clearly reflects the important effect of structural anisotropy on the property anisotropy. Therefore, the stress-induced structural anisotropy should also be considered in the performance design of glasses for their structural applications.

In summary, we propose the structural anisotropy measured by the high-energy XRD technique, as a unique tool to identify the mode of local non-affine deformation in various types of glass. By interpreting the features of the anisotropic PDF through the squared non-affine displacement observed in computer simulations, modes of the non-affine atomic rearrangements governing the plastic flow of glasses can be determined. The modes are different between MGs and other types of glass with directional covalent bonds. The plastic flow of MGs is localized, occurring through the stretching and contraction of atomic bonds in localized plastic-flow zones embedded in the elastic matrix. In covalent glasses, deformation occurs through the local rotation of molecules or chemical motifs, which is allowed in open network structures. Our results demonstrate that the stress-induced structural anisotropy serves as an effective tool to sort out different modes of the atomic-scale non-affine deformation process in glassy solids, and provide key information for understanding their microscopic deformation mechanism.

Online content

Any methods, additional references, Nature Portfolio reporting summaries, source data, extended data, supplementary information, acknowledgements, peer review information; details of author contributions and competing interests; and statements of data and code availability are available at https://doi.org/10.1038/s41567-023-02243-9.

References

1. Bourhis, E. L. *Glass: Mechanics and Technology* (John Wiley & Sons, 2014).
2. Ernsberger, F. M. Mechanical properties of glass. *J. Non-Cryst. Solids* **25**, 293–321 (1977).
3. Morgan, R. J. & O'Neal, J. E. The mechanical properties of polymer glasses. *Polym. Plast. Technol.* **5**, 173–197 (1975).
4. Schuh, C. A., Hufnagel, T. C. & Ramamurty, U. Mechanical behavior of amorphous alloys. *Acta Mater.* **55**, 4067–4109 (2007).
5. Greer, A. L., Cheng, Y. Q. & Ma, E. Shear bands in metallic glasses. *Mat. Sci. Eng. R* **74**, 71–132 (2013).
6. Yavari, A. R., Lewandowski, J. J. & Eckert, J. Mechanical properties of bulk metallic glasses. *MRS Bull.* **32**, 635–638 (2011).
7. Wondraczek, L. Overcoming glass brittleness. *Science* **366**, 804–805 (2019).
8. Hofmann, D. C. et al. Designing metallic glass matrix composites with high toughness and tensile ductility. *Nature* **451**, 1085–1089 (2008).
9. Sarac, B. & Schroers, J. Designing tensile ductility in metallic glasses. *Nat. Commun.* **4**, 2158 (2013).
10. Hirata, A. et al. Direct observation of local atomic order in a metallic glass. *Nat. Mater.* **10**, 28–33 (2011).
11. Chen, D. Z. et al. Fractal atomic-level percolation in metallic glasses. *Science* **349**, 1306–1310 (2015).
12. Yang, Y. et al. Determining the three-dimensional atomic structure of an amorphous solid. *Nature* **592**, 60–64 (2021).
13. Falk, M. L. The flow of glass. *Science* **318**, 1880–1881 (2007).
14. Cubuk, E. D. et al. Structure-property relationships from universal signatures of plasticity in disordered solids. *Science* **358**, 1033–1037 (2017).
15. Wang, Z., Sun, B. A., Bai, H. Y. & Wang, W. H. Evolution of hidden localized flow during glass-to-liquid transition in metallic glass. *Nat. Commun.* **5**, 5823 (2014).

16. Huang, P. Y. et al. Imaging atomic rearrangements in two-dimensional silica glass: watching silica's dance. *Science* **342**, 224–227 (2017).
17. Spaepen, F. A microscopic mechanism for steady state inhomogeneous flow in metallic glasses. *Acta Metall.* **25**, 407–415 (1976).
18. Argon, A. S. Plastic deformation in metallic glasses. *Acta Metall.* **27**, 47–58 (1979).
19. Falk, M. L. & Langer, J. S. Dynamics of viscoplastic deformation in amorphous solids. *Phys. Rev. E* **57**, 7192–7205 (1998).
20. Johnson, W. L. & Samwer, K. A universal criterion for plastic yielding of metallic glasses with a $(T/T_g)^{2/3}$ temperature dependence. *Phys. Rev. Lett.* **95**, 195501 (2005).
21. Liu, A. C. Y. et al. Local symmetry predictors of mechanical stability in glasses. *Sci. Adv.* **8**, eabn0681 (2022).
22. Schall, P., Weitz, D. A. & Spaepen, F. Structural rearrangements that govern flow in colloidal glasses. *Science* **318**, 1895–1899 (2007).
23. Laurati, M., Masshoff, P., Mutch, K. J., Egelhaaf, S. U. & Zaccone, A. Long-lived neighbors determine the rheological response of glasses. *Phys. Rev. Lett.* **118**, 018002 (2017).
24. Kong, D. J., Chen, W. R., Zeng, K. Q., Porcar, L. & Wang, Z. Localized elasticity governs the nonlinear rheology of colloidal supercooled liquids. *Phys. Rev. X* **12**, 041006 (2022).
25. Demkowicz, M. J. & Argon, A. S. High-density liquidlike component facilitates plastic flow in a model amorphous silicon system. *Phys. Rev. Lett.* **93**, 025505 (2004).
26. Wang, Y. et al. Tension–compression asymmetry in amorphous silicon. *Nat. Mater.* **20**, 1371–1377 (2021).
27. Zaccone, A. & Scossa-Romano, E. Approximate analytical description of the nonaffine response of amorphous solids. *Phys. Rev. B* **83**, 184205 (2011).
28. Ganguly, S., Sengupta, S. & Sollich, P. Statistics of non-affine defect precursors: tailoring defect densities in colloidal crystals using external fields. *Soft Matter* **11**, 4517–4526 (2015).
29. Ganguly, S., Sengupta, S., Sollich, P. & Rao, M. Nonaffine displacements in crystalline solids in the harmonic limit. *Phys. Rev. E* **87**, 042801 (2013).
30. DiDonna, B. A. & Lubensky, T. C. Nonaffine correlations in random elastic media. *Phys. Rev. E* **72**, 066619 (2005).
31. Popli, P., Kayal, S., Sollich, P. & Sengupta, S. Exploring the link between crystal defects and nonaffine displacement fluctuations. *Phys. Rev. E* **100**, 033002 (2019).
32. Nath, P. et al. On the existence of thermodynamically stable rigid solids. *Proc. Natl Acad. Sci. USA* **115**, 4322–4329 (2018).
33. Zaccone, A. & Terentjev, E. M. Disorder-assisted melting and the glass transition in amorphous solids. *Phys. Rev. Lett.* **110**, 178002 (2013).
34. Lemaître, A. & Maloney, C. Sum rules for the quasi-static and visco-elastic response of disordered solids at zero temperature. *J. Stat. Phys.* **123**, 415–453 (2006).
35. Palyulin, V. V. et al. Parameter-free predictions of the viscoelastic response of glassy polymers from non-affine lattice dynamics. *Soft Matter* **14**, 8475–8482 (2018).
36. Milkus, R. & Zaccone, A. Local inversion-symmetry breaking controls the boson peak in glasses and crystals. *Phys. Rev. B* **93**, 094204 (2016).
37. Hess, S. Shear-flow-induced distortion of the pair-correlation function. *Phys. Rev. A* **22**, 2844–2848 (1980).
38. Huang, G. R., Wu, B., Wang, Y. Y. & Chen, W. R. Characterization of microscopic deformation through two-point spatial correlation functions. *Phys. Rev. E* **97**, 012605 (2018).
39. Evans, D. J., Hanley, H. J. M. & Hess, S. Non-Newtonian phenomena in simple fluids. *Phys. Today* **37**, 26–35 (1984).
40. Wang, Z. et al. Fingerprinting molecular relaxation in deformed polymers. *Phys. Rev. X* **7**, 031003 (2017).
41. Dmowski, W., Iwashita, T., Chuang, C. P., Almer, J. & Egami, T. Elastic heterogeneity in metallic glasses. *Phys. Rev. Lett.* **105**, 205502 (2010).
42. Suzuki, Y., Haimovich, J. & Egami, T. Bond-orientational anisotropy in metallic glasses observed by X-ray diffraction. *Phys. Rev. B* **35**, 2162–2168 (1987).
43. Wang, H. et al. Nonaffine strains control ductility of metallic glasses. *Phys. Rev. Lett.* **128**, 155501 (2022).
44. Egami, T., Iwashita, T. & Dmowski, W. Mechanical properties of metallic glasses. *Metals* **3**, 77–113 (2013).
45. Dmowski, W. & Egami, T. Observation of structural anisotropy in metallic glasses induced by mechanical deformation. *J. Mater. Res.* **22**, 412–418 (2011).
46. Ott, R. T. et al. Anelastic strain and structural anisotropy in homogeneously deformed $Cu_{64.5}Zr_{35.5}$ metallic glass. *Acta Mater.* **56**, 5575–5583 (2008).
47. Choi, I. C. et al. Indentation size effect and shear transformation zone size in a bulk metallic glass in two different structural states. *Acta Mater.* **60**, 6862–6868 (2012).
48. Fan, Y., Iwashita, T. & Egami, T. How thermally activated deformation starts in metallic glass. *Nat. Commun.* **5**, 5083 (2014).
49. Maloney, C. E. & Lemaître, A. Amorphous systems in athermal, quasistatic shear. *Phys. Rev. E* **74**, 016118 (2006).
50. Miracle, D. B. A structural model for metallic glasses. *Nat. Mater.* **3**, 697–702 (2004).
51. Sheng, H. W., Luo, W. K., Alamgir, F. M., Bai, J. M. & Ma, E. Atomic packing and short-to-medium-range order in metallic glasses. *Nature* **439**, 419–425 (2006).
52. Lan, S. et al. A medium-range structure motif linking amorphous and crystalline states. *Nat. Mater.* **20**, 1347–1352 (2021).
53. Ye, J. C., Lu, J., Liu, C. T., Wang, Q. & Yang, Y. Atomistic free-volume zones and inelastic deformation of metallic glasses. *Nat. Mater.* **9**, 619–623 (2010).
54. Wang, W. H., Yang, Y., Nieh, T. G. & Liu, C. T. On the source of plastic flow in metallic glasses: concepts and models. *Intermetallics* **67**, 81–86 (2015).
55. Pan, D., Inoue, A., Sakurai, T. & Chen, M. W. Experimental characterization of shear transformation zones for plastic flow of bulk metallic glasses. *Proc. Natl Acad. Sci. USA* **105**, 14769–14772 (2008).
56. Sun, Y. H. et al. Flow-induced elastic anisotropy of metallic glasses. *Acta Mater.* **112**, 132–140 (2016).

Methods

Materials and sample preparation

Four types of glass, including MG ($Zr_{52.5}Cu_{17.9}Ni_{14.6}Al_{10}Ti_5$, Vit105 MG), polymer glass (PS), monatomic glass (amorphous Se) and oxide glass (B_2O_3), are chosen for this study. For MGs, ingots were prepared by weighing appropriate amounts of pure elements (purity, >99.95%) and then alloyed by arc melting in a Ti-gettered argon atmosphere. MG rods with a diameter of 2.5 mm were made by suck casting into a water-cooled Cu mould. The rods with the same diameter for the other three types of glass (PS, Se and B_2O_3) were prepared by casting the re-melted melts of powder or slices of the same composition into cold Cu moulds. All of the prepared rods were cut into cylinder-shaped samples with diameters of 2.5 mm and a length of 5.0 mm for compression and creep tests. Thermal properties of the prepared samples such as T_g were determined by a differential scanning calorimeter (PerkinElmer 8000) at a heating rate of 20 K min^{-1}. The amorphous structure of the samples was confirmed through XRD testing (Bruker D8 instrument, Cu Kα radiation).

Mechanical testing

Before compression and creep testing, all the cylindrical samples were pre-annealed at $0.9T_g$ in a vacuum annealing furnace for 8 h to reach a relaxed state. To determine the yield strength σ_y, the annealed samples were uniaxially compressed with a strain rate of 2.5×10^{-4} s^{-1} at $0.9T_g$ in a flowing argon environment. For each material, three samples were tested to confirm the repeatability. Creep experiments were conducted by uniaxially compressing the samples to $0.9\sigma_y$ and then held for 4 h using a loading controlling mode of the testing machine, at room temperature and high temperature. After thermo-creep, the samples were unloaded and drawn in cold water within 5 s to retain the deformed configuration as much as possible. The longitudinal and radial moduli of the crept samples were measured by nanoindentation tests on the polished cross section and longitudinal section of the cylindrical sample. On each section, 16 indentations in a 4 × 4 matrix with an interval space of 100 μm were loaded to a depth of 400 nm at a quasi-static loading rate.

Structure characterization

Structure characterization was carried out through high-energy XRD at the 6-ID beamline of the Advanced Photon Source, Argonne National Laboratory. A monochromatic X-ray beam with a wavelength of 0.12359 Å (100 keV) was used to obtain diffraction patterns in the transmission geometry. A two-dimensional stationary detector with 2,048 × 2,048 pixels and 200 μm × 200 μm pixel size was used to collect the diffraction pattern. The beam centre, detector tilt angles and distance between the sample and detector were calibrated using the CeO_2 powder standard. FIT2D software (version number: V17.006) was used to correct for dark current and to re-bin the data. The non-uniformity of the incident beam and detector response may cause an anisotropic diffraction signal. To reduce this effect, a flat-field calibration was conducted to ensure nearly perfect uniform illumination. Also, the dark signal for the detector was collected when the beam was off and subtracted from the sample signal to reduce any instrumental error. To improve the statistical results, the diffraction signal is collected for a long time before the detector reached the saturation limit, and the measurements were repeated several times until no further improvement was observed. After creep deformation, the cylindrical samples were rapidly quenched to room temperature to retain the anisotropic structure. Then, thin plates with a size of ~2.5 mm × 4.5 mm × 0.5 mm were cut from the central part of the annealed and crept samples along the loading axis for performing synchrotron XRD tests at room temperature. The XRD measurement was tested on a sample along two orientations: for the first measurement, the loading axis of the crept samples is parallel to the 'instrumental *z* axis' of the XRD measurement, which was defined as the P position. For the second measurement, the thin-plate samples were in-plane (*y*–*z* plane) rotated by 90° with the loading axis vertical to the '*z* axis', and is defined as the N position (Fig. 1a).

Atomistic simulations

We performed classical MD simulations of a model CuZr binary alloy based on the developed embedded-atom method[57], and a coarse-grained PS model[58] by LAMMPS code[47]. In the PS model, each styrene unit is coarse grained into four beads, with one representing the aliphatic moiety and three representing the phenyl ring. Each PS chain contains ten monomers, with the beads on each monomer connecting via the B-mapping method. For the mechanical property simulation, both systems contain 40,000 particles in a cubic box with the periodic boundary condition applied in every dimension. After identifying the yield stress for uniaxial compression at $0.8T_g$, we simulated the creep experiment by applying a constant stress along the '*y* axis' at $0.65\sigma_y$ for a time interval of 40 ns for CuZr and 100 ns for PS at the same reduced temperature. Then, the pressure was released. After stress retracting, the shape of the sample does not return to the original one, with a portion of residual strain sustained. Thus, the involvement of plastic deformation for particles after the creep was characterized by the squared non-affine displacement[19]. Configuration information was collected after short-time relaxation, when the system reached the steady state, without showing any notable energy drift.

Data availability

The data that support the findings of this study are available via Figshare at https://doi.org/10.6084/m9.figshare.23515368. Source data are provided with this paper.

Code availability

Code data are available from the corresponding authors upon reasonable request.

References

57. Mendelev, M. I. et al. Development of suitable interatomic potentials for simulation of liquid and amorphous Cu-Zr alloys. *Philos. Mag.* **89**, 967–987 (2009).
58. Rossi, G., Monticelli, L., Puisto, S. R., Vattulainen, I. & Ala-Nissila, T. Coarse-graining polymers with the MARTINI force-field: polystyrene as a benchmark case. *Soft Matter* **7**, 698–708 (2011).

Acknowledgements

This research was supported by the National Key Research and Development Plan with grant no. 2018YFA0703603 (B.S.); the Guangdong Major Project of Basic and Applied Basic Research of China with grant nos. 2019B030302010 (W.W.) and 2020B1515120092 (B.S.); the National Natural Science Foundation of China (NSFC) with grant nos. 52192601 (H.B.), 52192602 (B.S.), 61888102 (W.W.) and 52001272 (Y.T.); and the Strategic Priority Research Program of Chinese Academy of Sciences with grant no. XDB30000000 (W.W.). W.D. and T.E. were supported by the US Department of Energy, Office of Science, Basic Energy Sciences, Materials Sciences and Engineering Division. H.P. acknowledges the computer resources provided by High Performance Computing Cluster (HPC) of Central South University.

Author contributions

H.B. and B.S. conceived and supervised the project. J.D. prepared the materials and performed the mechanical and thermal experiments. H.P. performed the MD simulations. H.W., Y.T. and W.D. performed the high-energy XRD experiments. J.D., Y.T., H.P., Y.W. and B.S. performed the data analysis and wrote the manuscript with input from all the other co-authors. T.E., W.W. and H.B. discussed the results and revised the manuscript.

Competing interests
The authors declare no competing interests.

Additional information
Supplementary information The online version contains supplementary material available at https://doi.org/10.1038/s41567-023-02243-9.

Correspondence and requests for materials should be addressed to Hailong Peng, Yang Tong, Baoan Sun or Haiyang Bai.

Peer review information *Nature Physics* thanks the anonymous reviewers for their contribution to the peer review of this work.